Ukrainian Journal of Physical Optics
ISSUE 4
2025

MECHANISM FOR 32-FOLD FREQUENCY MULTIPLICATION TERAHERTZ WAVE GENERATION BASED ON TWO DUAL-PARALLEL AND ONE CASCADED MZMS WITHOUT FILTERING FOR HIGH-FREQUENCY COMMUNICATIONS

YANG CUI[1], DONGFEI WANG[2,3], XIANGQING WANG[1,4,5]*, XIAOKUN YANG[2,3,4], JIAHUI WANG[1], DAISHENG ZHANG[1]

[1] School of Physics and Electronic Engineering, Fuyang Normal University, Fuyang, 236037, China
[2] School of Artificial Intelligence, Wuhan Technology and Business University, Wuhan, 430065, China
[3] School of Electronic Information, Nanchang Institute of Technology, Nanchang, China
[4] Advanced Cryptography and System Security Key Laboratory of Sichuan Province, Chengdu, China
[5] Henan Key Laboratory of Visible Light Communications, Zhengzhou, China
*Corresponding author: wxqing@fynu.edu.cn

Received: 16.07.2025

Abstract. This paper presents a scheme for generating 32×frequency millimeter waves through secondary modulation without filters, based on five Mach-Zehnder modulators (MZMs). The system is driven by a 5 GHz radio frequency (RF) signal. Each of the two dual-parallel MZMs contains two MZMs working in parallel. The first modulation produces an 80 GHz RF signal for the second modulation. After passing through a direct current blocking module, a cascaded MZM performs secondary modulation to generate ±16th-order optical sidebands. Finally, 32×frequency multiplication is achieved through the beat frequency at the photodetector. Theoretical analysis and simulation experiments indicate that the system's optical sideband suppression ratio is 53.33 dB, and the RF sideband suppression ratio is 47.98 dB. These consistent results validate the scheme's feasibility. The impact of non-ideal factors of MZMs on system stability is examined via simulation, and their tolerable ranges are provided. Lastly, simulation results show that the bit error rate remains below 10^{-9} when transmitting 2.5 Gbps baseband-modulated millimeter wave signals over 15 km of optical fiber. This scheme features a simple structure and a high-frequency multiplication factor, offering promising applications in millimeter wave technology.

Keywords: millimeter-wave, Mach-Zehnder modulator, radio frequency sideband rejection ratio, optical sideband rejection ratio, millimeter-wave optical fiber transmission, 32-fold frequency multiplication
UDC: 621.396.9
DOI: 10.3116/16091833/Ukr.J.Phys.Opt.2025.04032

1. Introduction

With the rapid development of video streaming, cloud computing, and the Internet of Things – especially driven by advances in 5G and upcoming 6G technologies – the need for high-speed, high-capacity communication solutions is increasingly rising [1]. Traditional wireless systems operating in low-frequency bands now struggle to keep up with these growing demands. Wireless communication carrier frequencies have shifted into the millimeter-wave (MMW) and terahertz (THz) ranges [2-5]. In recent years, the MMW and THz bands have attracted attention because of their abundant frequency resources and are seen as strong drivers for 5G/6G [6,7]. Traditional electrical-domain millimeter-wave generation methods are limited by the bandwidth of electronic devices, making it difficult to generate MMW signals with frequencies above

100 GHz [8]. However, generating MMW in the optical domain can effectively overcome this limitation and provides advantages such as flexible frequency tuning and easy integration with optical fiber networks, making it a key technology for MMW generation. Currently, the main methods proposed for producing MMW in the optical domain include direct modulation [9], optical heterodyning [10], external modulation [11-14], mode-locked lasers [15], up-conversion modulation [16,17], stimulated Brillouin scattering (SBS) [18], and four-wave mixing (FWM) [19]. Although direct and up-conversion modulation have simple structures, the frequencies of the generated signals are limited. Schemes using FWM and SBS technologies to generate MMW have complex structures and limited frequency multiplication factors (FMFs). Among these, the external modulation method offers advantages such as a high modulation bandwidth, high tunability, high-frequency responsiveness, high spectral purity of the generated signals, and good system stability, making it the primary method for generating optical millimeter waves. External modulators are typically used with filters or wavelength-selective switches to achieve frequency multiplication effects, such as 2× [20, 21], 4× [22, 23], 6× [24, 25], and even 8× [26]. However, generating higher-frequency MMW requires more complex schemes that utilize higher-order harmonic frequencies. Additionally, these schemes demand optical filters or wavelength-selective switches to be adjusted to different frequencies based on actual conditions to satisfy varying frequency requirements, which significantly limits the tunable range and adaptability of the generated signals. In Ref. [27], a new method for producing 6× MMW using a dual-parallel Mach-Zehnder modulator (DPMZM) is proposed, with a maximum output power of 32 dB and a simple structure, but it features a low-frequency multiplication factor. Ref. [28] achieves filter-free 12×frequency multiplication based on two parallel Mach-Zehnder modulators (MZMs), further increasing the multiplication factor, but the spectral purity of the generated signal is low. Ref. [29] proposes a 16×frequency multiplication scheme using an MZM for secondary modulation, followed by cascading a fiber Bragg grating (FBG). Still, the presence of FBG increases system complexity and significantly reduces its tunability. Similarly, Ref. [30] achieves 40× frequency multiplication using a DPMZM cascaded with an MZM and a Bragg grating (FBG). Although the generated signal has high purity, the FBG reduces the system's tunability. Ref. [31] proposes a filter-free scheme for generating 18× MMW using three cascaded MZMs, with an optical sideband suppression ratio (*OSSR*) and radio-frequency sideband suppression ratio (*RFSSR*) of 31.5 dB and 32.02 dB, respectively, but the purity and multiplication factor of the MMW signal still need improvement. Ref. [32] presents a filter-free 24× MMW generation scheme based on two cascaded DPMZMs, but the *RFSSR* is only 26 dB. Refs. [33,34] propose a structure using eight parallel MZMs to generate 32× MMW, but excessive modulators lead to high losses, severely reducing signal power and sensitivityRef. [35] proposes a filter-free 32×MMW generation scheme using four DPMZMs, but *OSSR* is only 40 dB. Ref. [36] proposes a filterless 32-fold frequency MMW generation scheme using two cascaded dual-parallel DPMZMs. The simulation experiment results of its *OSSR* and *RFSSR* are 53.53 dB and 47.33 dB, respectively. However, it requires the use of polarization devices, which can affect reliability in actual deployment.

To compare our method with other MZM-based methods, we list the main parameters in Table 1. To address the issues mentioned above and enhance the system's frequency multiplication factor without compromising its tunability, this paper proposes a scheme for generating 32× high-purity MMW through secondary modulation of signals using five MZMs, without any filters, and analyzes how parameter variations affect system performance. The

paper is divided into five sections. The second section introduces the scheme's structure and principles. The third section presents simulation experiments to explore the influence of various non-ideal factors on system stability. The fourth section verifies the system's transmission performance. Finally, the fifth section concludes the paper.

Table 1. Comparison of the proposed methodology with previously reported works.

Ref.	Architecture	FMF	*OSSR*, dB	*RFSSR*, dB
[27]	Used an integrated dual-polarization modulator	6	38	32
[28]	Used two nested MZMs	12	37	38
[29]	Used three cascaded MZMs	16	54.86	47.9
[30]	Used a DPMZM cascaded with an MZM	40	25.61	20
[31]	Used three cascaded MZMs	18	31.5	32.02
[32]	Used two cascaded DPMZMs	24	33	26
[33,34]	Used eight parallel MZMs	32	61.42	55.27
[35]	Used two parallel DPMZMs and two cascaded DPMZMs	32	40	46
[36]	Used two cascaded dual-parallel DPMZMs	32	53.53	47.33
Proposed in the present work	Two Dual-Parallel and One Cascaded MZMs	32	53.33	47.98

2. Structural design and program principles of MZM-based generation of 32-tupling MMW

2.1. Structure of the setup

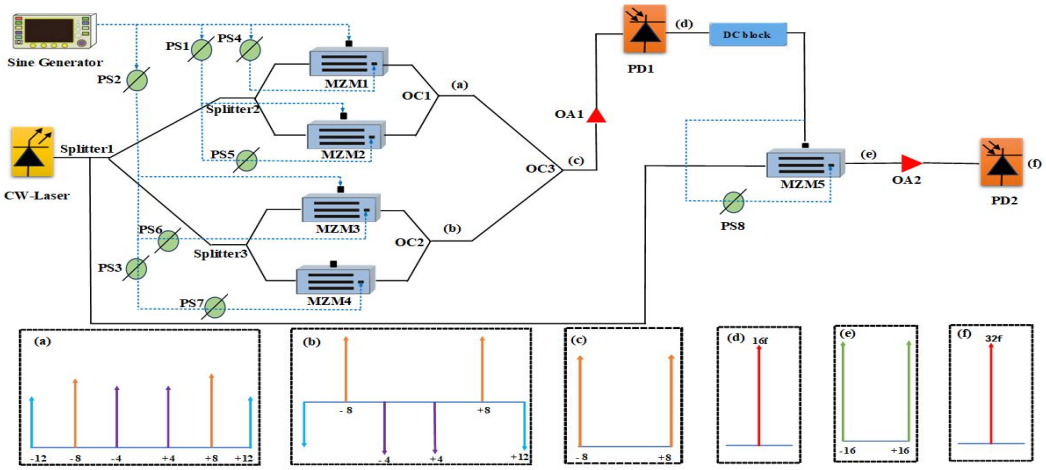

Fig. 1. Schematic diagram of the 32× frequency multiplication scheme for millimeter-wave generation. PS - phase shifter; OA - optical amplifier; PD – photodiode; Splitter – optical beam splitter; OC – optical coupler (the DC block prevents DC signals from passing through while allowing high-frequency millimeter-wave signals to transmit without attenuation). In the insets: diagram (a) shows the output spectrum of DPMZM1, diagram (b) shows the output spectrum of DPMZM2, diagram (c) shows the output spectrum of the first modulation, diagram (d) shows the 80 GHz millimeter-wave signal generated by the first modulation, diagram (e) shows the output spectrum of the second modulation, and diagram (f) shows the 160 GHz millimeter-wave signal generated by the second modulation (16f and 32f are abbreviations for the 80 and 160 GHz millimeter-wave signals, respectively).

Fig. 1 shows the schematic diagram of a system based on two dual-parallel and one cascaded MZMs. The system includes a continuous-wave laser (CW laser), an RF sine generator, eight electrical phase shifters (PSs), MZMs labeled as MZMi (i = 1, 2, 3, 4, 5), an optical beam splitter, an optical coupler, a DC block, OAs labeled OA1 and OA2, and two photodetectors (PD1 and PD2). Four of the MZMs are divided into two groups; each group has two parallel MZMs, which function as two DPMZMs connected in parallel. The initial phase difference between the RF signals of MZM1 and MZM2 (in DPMZM1) is π/2, the phase difference between MZM3 and MZM4 (in DPMZM2) is π/2, and the overall phase difference between the RF signals driving DPMZM1 and DPMZM2 is π/4. The optical wave from the CW laser is injected into DPMZM1 and DPMZM2, where it is modulated by the RF drive signals. The outputs from DPMZM1 and DPMZM2 are ±4th, ±8th, and ±12th-order optical sidebands, which are combined by the optical coupler to isolate only the ±8th-order sidebands. OA1 first amplifies these optical signals and then injects them into PD1 to generate 80 GHz RF signals. These RF signals are then separated from DC by a DC block and used as the RF drive signal for MZM5. A CW laser supplies the optical carrier for MZM5. The MZM5 outputs ±16th-order optical sidebands, which are amplified by OA2 and fed into PD2 to produce a 160 GHz electrical signal – 32 times the original RF frequency of 5 GHz.

2.2. Theoretical derivation procedure

2.2.1. First-order modulation principle. The optical wave from the CW laser can be expressed as: $E_{in} = E_0 \exp(j\omega_c t)$, where E_0 and ω_0 are the amplitude and angular frequency of the optical carrier, respectively. The RF drive signals loaded on the two arms of the MZM are $V_1 = V_{RF}\cos(\omega_{RF}t)$ and $V_2 = V_{RF}\cos(\omega_{RF}t)$, where V_{RF} and ω_{RF} are the voltage amplitude and angular frequency of the RF signals, respectively. Assuming that both MZM1 and MZM2 operate at the maximum transmission point (MATP) and the initial phase difference of the RF drive signals between the two MZMs is π/2. The output of MZM1 can be expressed as:

$$\begin{aligned} E_{MZM1} &= \alpha E_0 e^{j\left[\omega_0 t + m\cos(\omega_m t)\right]} \\ &\quad + \alpha E_0 e^{j\left[\omega_0 t + m\cos(\omega_m t + \pi)\right]} \\ &= \alpha E_0 e^{j\omega_0 t}\left[\sum_{n=-\infty}^{\infty} j^n J_n(m) e^{jn\omega_m t}\left[1 + (-1)^n\right]\right] \\ &= \alpha E_0 e^{j\omega_0 t} 2\left[\sum_{n=-\infty}^{\infty} (-1)^n J_{2n}(m) e^{j2n\omega_m t}\right] \end{aligned} \tag{1}$$

In Eq. (1), $m = \frac{V_{RF}\pi}{V_\pi}$ is the modulation index of the MZM, V_π is the half-wave voltage of the MZM, α is the loss of the MZM, and $J_n(m)$ is the first-type Bessel function. The Jacobi–Anger expansion $e^{jx\cos\theta} = \sum_{n=-\infty}^{\infty} j^n j_n(x) e^{jn\theta}$ is utilized in Eq.(1). The output of MZM1 is ±2n order optical sidebands, where *n* is an integer. By setting the initial phase of the RF drive signal loaded into MZM2 to have a delay φ_1 with respect to the initial phase of MZM1, the output signal of DPMZM1 can be expressed as follows:

$$
\begin{aligned}
E_{DPMZM1} &= E_{MZM1} + E_{MZM2} \\
&= \alpha E_0 e^{j\omega_0 t}\left[\sum_{n=-\infty}^{\infty}(-1)^n J_{2n}(m)e^{j2n\omega_m t} + \sum_{n=-\infty}^{\infty}(-1)^n J_{2n}(m)e^{j2n(\omega_m t+\varphi_1)}\right] \\
&= \alpha E_0 e^{j\omega_0 t}\left[\sum_{n=-\infty}^{\infty}(-1)^n J_{2n}(m)e^{j2n\omega_m t}\left(1+e^{j2n\varphi_1}\right)\right]
\end{aligned}
\tag{2}
$$

When $\varphi_1 = \pi/2$, $\left[1+e^{j2n(\pi/2)}\right]=\left[1+(-1)^n\right]$, we can see that in Eq. (2) only the even light sidebands are preserved and the odd sidebands are suppressed; accordingly, Eq.(2) can be simplified as follows:

$$
E_{DPMZM1} = \alpha E_0 e^{j\omega_0 t} 4\left[\sum_{n=-\infty}^{\infty} J_{4n}(m)e^{j4n\omega_m t}\right]. \tag{3}
$$

Thus, the output of DPMZM1 consists of ±4n order optical sidebands.

Since DPMZM1 and DPMZM2 have the same structure, by setting the initial phase of the RF drive signal loaded into DPMZM2 to have a delay φ_2 relative to the initial phase of DPMZM1, the output signal of the two parallel DPMZMs is

$$
\begin{aligned}
E_{out1} &= E_{DPMZM1} + E_{DPMZM2} \\
&= \alpha E_0 e^{j\omega_0 t} 4\left[\sum_{n=-\infty}^{\infty} J_{4n}(m)e^{j4n\omega_m t} + \sum_{n=-\infty}^{\infty} J_{4n}(m)e^{j4n(\omega_m t+\varphi_2)}\right] \\
&= \alpha E_0 e^{j\omega_0 t} 4\left[\sum_{n=-\infty}^{\infty} J_{4n}(m)e^{j4n\omega_m t}\left(1+e^{j4n\varphi_2}\right)\right]
\end{aligned}
\tag{4}
$$

When $\varphi_2 = \pi/4$, $\left[1+e^{j4n(\pi/4)}\right]=\left[1+(-1)^n\right]$, we can see that only the even light sidebands are preserved in Eq. (4) and the odd sidebands are suppressed; accordingly, Eq. (4) can be simplified as follows:

$$
\begin{aligned}
E_{out1} &= \alpha E_0 e^{j\omega_0 t} 8\left[\sum_{n=-\infty}^{\infty} J_{8n}(m)e^{j8n\omega_m t}\right] \\
&= \alpha E_0 e^{j\omega_0 t} 8\left[\begin{array}{l} J_0(m) + J_{-8}(m)e^{-j8\omega_m t} + J_8(m)e^{j8\omega_m t} \\ +J_{-16}(m)e^{-j16\omega_m t} + J_{16}(m)e^{j16\omega_m t} + \ldots \end{array}\right] \\
&= \alpha E_0 e^{j\omega_0 t} 8\left[J_0(m) + 2J_8(m)\cos(8\omega_m t) + 2J_{16}(m)\cos(16\omega_m t) + \ldots\right]
\end{aligned}
\tag{5}
$$

In Eq. (5), harmonic terms for $n \geq 2$ are relatively small and can be neglected.

After being combined by an optical coupler, DPMZM1 and DPMZM2 mainly output 0, ±8, and ±16 order optical variable bands. According to the Bessel function of the first kind, when m = 8.6550877606, $J_0(m)$ and $J_{16}(m)$ reach their minimum values while $J_8(m)$ reaches its maximum value, and the 0th-order optical sideband as well as the ±16th-order optical sidebands can be well suppressed. When m=8.6550877606, $J_0(m)=3.453\times10^{-4}$, $J_8(m)=0.2819$, $J_{16}(m)=0.0002317$ and since $J_0(m)$ and $J_{16}(m)$ are too small to be neglected, then Eq. (5) can be simplified as follows:

$$
E_{\text{out}1} = 16\alpha E_0 e^{j\omega_0 t}\left[J_8(m)\cos(8\omega_m t)\right]. \tag{6}
$$

Therefore, the outputs of these two groups of MZMs are ±8$^{\text{th}}$-order optical sidebands. When

the outputs of the two groups of MZMs are input to PD1 to realize photoelectric conversion, the output of PD1 can be expressed as:

$$I(t) \propto R\left|E_{out1}\right|^2 = R\alpha^2\left\{E_0 e^{j\omega_0 t} 2\left[\sum_{n=-\infty}^{\infty} J_{8n}(m) e^{j8n\omega_m t}\right]\right\}^2$$
$$= R\alpha^2 E_0^2 4\left\{\begin{array}{l}\left[\begin{array}{l}J_0(m)^2 + 2J_8(m)^2 + \\ 2J_{16}(m)^2 + 2J_{24}(m)J_{24}(m)\end{array}\right]\cos(0\omega_m t) \\ +2\left[\begin{array}{l}2J_0(m)J_8(m) + 2J_8(m)J_{16}(m) \\ +J_{16}(m)J_{24}(m) + J_{24}(m)J_{16}(m)\end{array}\right]\cos(8\omega_m t) \\ +2\left[2J_0(m)J_{16}(m) + J_8^2(m) + 2J_8(m)J_{24}(m)\right]\cos(16\omega_m t) \\ +2\left[2J_0(m)J_{24}(m) + 2J_8(m)J_{16}(m)\right]\cos(24\omega_m t) + \ldots\end{array}\right\}, \quad (7)$$

where n=0, 1, 2, 3, and R is the responsivity of PD1.

Since, $J_{24}(m) = 1.402 \times 10^{-9}$ and is too small it can be ignored, then Eq. (7) can be simplified as follows:

$$I(t) \propto R\alpha^2 E^2{}_0 J_8^2(m)\cos(16\omega_m t) \propto J_8^2(m)\cos(16\omega_m t). \quad (8)$$

According to the definition of OSSR:

$$OSSR_{(P_8/P_0)} = 10\log\left[\left(\frac{J_8(m)}{J_0(m)}\right)^2\right]_{m=8.655} = 58.23\text{dB}.. \quad (9)$$

According to the definition of RFSSR

$$RFSSR = 10\log\left\{\frac{2\left[2J_0(m)J_{16}(m) + J_8^2(m) + 2J_8(m)J_{24}(m)\right]}{2\left[2J_0(m)J_{24}(m) + 2J_8(m)J_{16}(m)\right]}\right\}^2 = 55.68\text{dB}. \quad (10)$$

2.2.2. The principle of the second-order modulation. The 80 GHz RF signal obtained from the first modulation and the optical signal generated by the CW laser are used as the RF drive signal and the optical wave, respectively, for the second modulation. They are both injected into MZM5 for the second modulation. By setting the MZM5 to operate at the minimum transmission point, the output signal from the MZM5 can be represented as:

$$E_{MZM5} = \alpha\frac{E_{in}}{2}\left[e^{j\varphi_1} + e^{j\varphi_2}\right]$$
$$= \frac{\alpha E_{in}}{2}\left[e^{j\pi\frac{\left(V_{DC1} + J_8^2(m)\cos(16\omega_m t + \theta_1)\right)}{V_\pi}} + e^{j\pi\frac{\left(V_{DC2} + J_8^2(m)\cos(16\omega_m t + \theta_2)\right)}{V_\pi}}\right]$$
$$= \frac{\alpha E_{in}}{2}\left[e^{j\pi\left[\frac{V_{DC1}}{V_\pi} + \frac{J_8^2(m)}{V_\pi}\cos(16\omega_m t + \theta_1)\right]} + e^{j\pi\left[\frac{V_{DC2}}{V_\pi} + \frac{J_8^2(m)}{V_\pi}\cos(16\omega_m t + \theta_2)\right]}\right]$$
$$= \frac{\alpha E_{in}}{2}e^{j\pi\left[\frac{V_{DC1} + V_{DC2}}{2V_\pi}\right]}\left[\begin{array}{l}e^{j\pi\left[\frac{V_{DC1} - V_{DC2}}{2V_\pi}\right]}e^{j\pi\frac{J_8^2(m)}{V_\pi}\cos(16\omega_m t + \theta_1)} \\ +e^{-j\pi\left[\frac{V_{DC1} - V_{DC2}}{2V_\pi}\right]}e^{j\pi\frac{J_8^2(m)}{V_\pi}\cos(16\omega_m t + \theta_2)}\end{array}\right] \quad (11)$$

$$= \frac{\alpha E_{in}}{2} e^{j\pi\left[\frac{V_{DC1}+V_{DC2}}{2V_\pi}\right]} \left[\begin{array}{l} e^{j\pi\left(\frac{V_{DC1}-V_{DC2}}{2V_\pi}\right)} \sum_{n=-\infty}^{n=+\infty} (j)^n J_n\left(\frac{\pi J_8^2(m)}{V_\pi}\right) e^{jn(16\omega_m t+\theta_1)} + \\ e^{-j\pi\left(\frac{V_{DC1}-V_{DC2}}{2V_\pi}\right)} \sum_{n=-\infty}^{n=+\infty} (j)^n J_n\left(\frac{\pi J_8^2(m)}{V_\pi}\right)^{jn(16\omega_m t+\theta_2)} \end{array} \right]$$

$$= \frac{\alpha E_{in}}{2} e^{j\pi\left[\frac{V_{DC1}+V_{DC2}}{2V_\pi}\right]} \sum_{n=-\infty}^{n=+\infty} (j)^n J_n\left(\frac{\pi J_8^2(m)}{V_\pi}\right) e^{jn(16\omega_m t)} \quad (11)$$

$$\times e^{j\frac{n(\theta_1+\theta_2)}{2}} \left[e^{j\pi\left(\frac{V_{DC1}-V_{DC2}}{2V_\pi}\right)} e^{j\frac{n(\theta_1-\theta_2)}{2}} + e^{-j\pi\left(\frac{V_{DC1}-V_{DC2}}{2V_\pi}\right)} e^{-j\frac{n(\theta_1-\theta_2)}{2}} \right] \quad \text{(continued)}$$

$$= \frac{\alpha E_{in}}{2} e^{j\pi\left[\frac{V_{DC1}+V_{DC2}}{2V_\pi}\right]} \sum_{n=-\infty}^{n=+\infty} J_n(K) e^{jn\left(16\omega_m t+\frac{\theta_1+\theta_2}{2}+\frac{\pi}{2}\right)}$$

$$\times \cos\left[\pi\left(\frac{V_{DC1}-V_{DC2}}{2V_\pi}\right)+\frac{n(\theta_1-\theta_2)}{2}\right]$$

where θ_1 and θ_2 are the phases of the upper and lower arms of MZM5, respectively, and V_{DC1} and V_{DC2} are the voltages of the upper arm and the lower arm of MZM5, respectively. When $V_1(t) = J_8^2(m)\cos(16\omega_m t + \theta_1)$, $V_2(t) = J_8^2(m)\cos(16\omega_m t + \theta_2)$, $\varphi_1 = \pi V_1(t)/V_\pi$, $\varphi_2 = \pi V_2(t)/V_\pi$, $K = \pi J_8^2(m)/V_\pi$ when $\theta_1 - \theta_2 = -\pi$, $V_{DC1} = 4\,\text{V}$, $V_{DC2} = 0\,\text{V}$ the Eq. (11) can be simplified as follows:

$$E_{MZM5} = \frac{\alpha E_{in}}{2} e^{j\frac{\pi}{2}} \sum_{n=-\infty}^{n=+\infty} J_n(K) e^{jn(16\omega_m t+\pi)} \cos\left[\frac{(n-1)\pi}{2}\right]$$

$$= \frac{\alpha E_{in}}{2} \left[\begin{array}{l} -2J_1(K)\cos\left(16\omega_m t+\pi-\frac{\pi}{2}\right)+2J_3(K)\cos 3\left(16\omega_m t+\pi-\frac{\pi}{2}\right)- \\ 2J_5(K)\cos 5\left(16\omega_m t+\pi-\frac{\pi}{2}\right) \end{array} \right]. \quad (12)$$

From Eq. (12), it can be seen that the main components of the MZM5 output signal are the ±16th order, ±48th order , and ±80th order sidebands, whose amplitudes are related to $J_1(K)$, $J_3(K)$ and $J_5(K)$. $J_1(0.221403742)$=0.1118 , $J_3(0.221403742)$=0.0002 and $J_5(0.221403742)$=1.285×10^{-7}, so the ±16th order sidebands are the main sidebands. In Eq. (12), when *n* is even, the cosine terms are all zero, so *n* can only take odd values. When *n* = 1, ±16th-order optical sidebands are generated; when *n* = 3, ±48th-order optical sidebands are generated; and when *n* = 5, ±80th-order optical sidebands are generated.

According to the definition of *OSSR*, we can get:

$$OSSR = 10\log\left[\left(\frac{J_1(K)}{J_3(K)}\right)^2\right] = 54.9\,\text{dB}. \quad (13)$$

By injecting ±16th order, ±48th order, and ±80th order sidebands into PD2 for photoelectric conversion, the output of PD2 can be expressed as:

$$I(t)\propto R\left|E_{MZM5}\right|^2=R\alpha^2\left\{\frac{E_{in}}{2}e^{j\frac{\pi}{2}}\sum_{n=-\infty}^{n=+\infty}J_n(K)e^{jn(16\omega_m t+\pi)}\cos\left[\frac{(n-1)\pi}{2}\right]\right\}^2$$
$$=R\frac{\alpha^2E_{in}^2}{4}\begin{Bmatrix}2\left[-J_1^2(K)-J_3^2(K)-J_5^2(K)\right]\\+2\begin{bmatrix}J_1^2(K)+2J_1(K)J_3(K)+\\2J_3(K)J_5(K)\end{bmatrix}\cos\left(32\omega_m t+\frac{\pi}{2}\right)\\-2\left[-2J_1(K)J_3(K)-2J_1(K)J_5(K)\right]\cos\left(64\omega_m t+\frac{\pi}{2}\right)+\\2\left[2J_1(K)J_5(K)+J_3^2(K)\right]\cos\left(96\omega_m t+\frac{\pi}{2}\right)\\-4J_3(K)J_5(K)\cos\left(128\omega_m t+\frac{\pi}{2}\right)\end{Bmatrix}, \quad (14)$$

where R is the responsivity of PD2, $J_1(0.221403742)=0.1118$, $J_3(0.221403742)=0.0002$ and $J_5(0.221403742)=1.285\times10^{-7}$. Formula (14) can be simplified as follows:

$$I(t)\propto R\alpha^2\frac{E_{in}^2}{2}J_1^2(K)\cos\left(32\omega_m t+\frac{\pi}{2}\right). \quad (15)$$

According to the definition of *RFSSR*

$$RFSSR=10\log\left[\left(\frac{2\left[J_1^2(K)+2J_1(K)J_3(K)+2J_3(K)J_5(K)\right]}{2\left[-2J_1(K)J_3(K)-2J_1(K)J_5(K)\right]}\right)^2\right]=48.96\text{ dB}. \quad 16)$$

3. Simulation experiments

The accuracy of the scheme is demonstrated through mathematical calculations and will be further confirmed by simulation experiments. First, the system's schematic diagram is constructed on the simulation platform OptiSystem based on Fig. 1. Second, the parameters for each component are set according to the results of theoretical derivation. The effects of parameter variations on the system's stability under non-ideal conditions are examined through simulation. MZM1~MZM4 operate at the maximum transmission point, while MZM5 operates at the minimum transmission point. The parameter settings for each component in the simulation system are listed in Table 2.

Table 2. The main parameters used in the simulation.

Devices	Parameters	Values
1	2	3
CW Laser	Frequency	193.1 THz
	line width	10 MHz
	Power	20 dBm
Sine generator	Frequency	5 GHz
	Amplitude	11.02 V
PS1	Phase shift	90°
PS2	Phase shift	45°
PS3	Phase shift	90°
PS4~ PS8	Phase shift	180°

1	2	3
OA1	Optical amplifier	23 dB
OA2	Optical amplifier	10dB
MZM1~MZM4	Half-voltage	4 V
	Extinction ratio	60 dB
	Insertion loss	5 dBm
MZM5	Half-voltage	4 V
	Extinction ratio	80 dB
	Insertion loss	5 dBm
PD	Responsivity	0.6 A/W
	Dark current	10 nA

3.1. System output spectrum analysis. Fig. 2 shows the output spectrograms of DPMZM1 and the first modulation; from Fig. 2a, it is clear that the variable light bands output from DPMZM1 contain only ±4th order, ±8th order, and ±12th order sidebands. From Fig. 2b, it is evident that when the phase difference between the RF drive signals of DPMZM1 and DPMZM2 is 45°, the ±4th-order and ±12th-order optical sidebands are effectively suppressed. Only the ±8th-order optical sidebands remain, with an OSSR of 57.97 dB, close to the calculated value of 58.23 dB.

Fig. 3 displays the signal spectra from PD1 and MZM5. As seen in Fig. 3a, the spectrum from PD1 has a frequency of 80 GHz, which acts as the RF drive signal for MZM5, with an RF SSR of up to 54.96 dB. In Fig. 3b, the optical sidebands output by MZM5 are mainly the

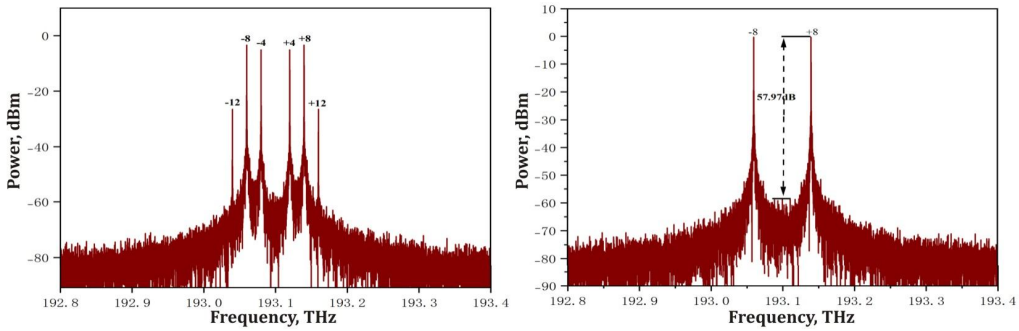

(a) (b)

Fig. 2. (a) DPMZM1 output spectrum. (b) First modulation output spectrum.

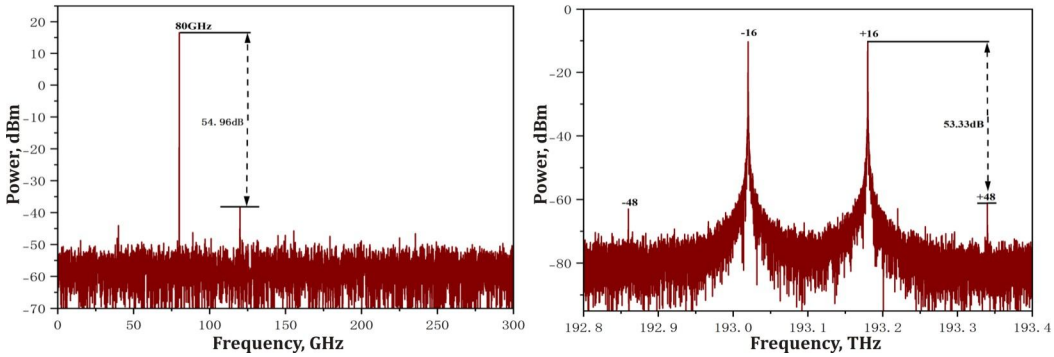

(a) (b)

Fig. 3. Output spectrum of PD1 after detection (a) and output spectrum of MZM5 (b).

±16th-order and ±48th-order sidebands, with an OSSR of 53.33 dB. Fig. 4 shows the output spectrum after PD2 detection. From Fig. 4, it is clear that PD2 detects the ±16th-order optical sideband from MZM5, producing a 160 GHz signal with an RFSSR of 47.98 dB. This scheme achieves generation of a 32-times frequency-multiplied millimeter-wave signal using two double-parallel MZMs and one cascaded MZM, with fewer external modulators than reference [33].

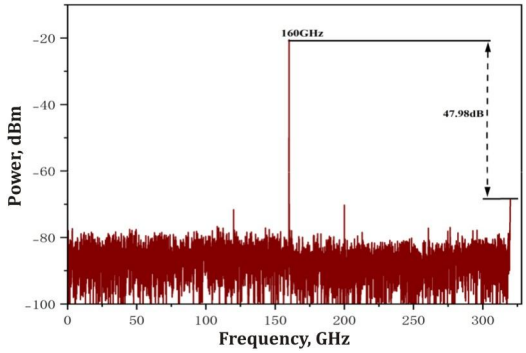

Fig. 4. Output spectrum after PD2 detection.

3.2. Impact of non-ideal factors on signal performance. In the theoretical derivation process and simulation experiments above, the device parameters are analyzed based on theory and assumed to be ideal. However, in real-world engineering applications, limitations in the device fabrication process and the influence of the surrounding environment cause these parameters to deviate from their ideal values. This deviation inevitably affects the OSSR and RFSSR of the generated signals. In this paper, we examine how the OA1 gain, the half-wave voltage, the extinction ratio, the modulation index, and the DC offset drift influence the OSSR and RFSSR of the signals, and we determine the tolerance ranges for each parameter bias under various factors.

3.2.1. Effect of OA1 gain. The gain of OA1 influences the amplitude of the 16th harmonic of the RF signal generated in PD1, which in turn affects the modulation index of the second modulation and consequently impacts the *OSSR* and *RFSSR* of the generated signal. The system is designed with OA1 gain set to 23 dB. The relationship between *OSSR*, *RFSSR*, and OA1 gain is derived from scan parameter experiments shown in Fig. 5, where the gain varies between 11 dB and 35 dB. When OA1 gain is 10 dB below the design value (a deviation of 43.48%), the *OSSR* drops to 52.29 dB and *RFSSR* decreases to 15.14 dB. Conversely, when it is 10 dB above the design value (same deviation percentage), the *OSSR* reduces to 15.2 dB and *RFSSR* falls to 21.56 dB. In both cases, the performance requirements for the public transmission link are still met.

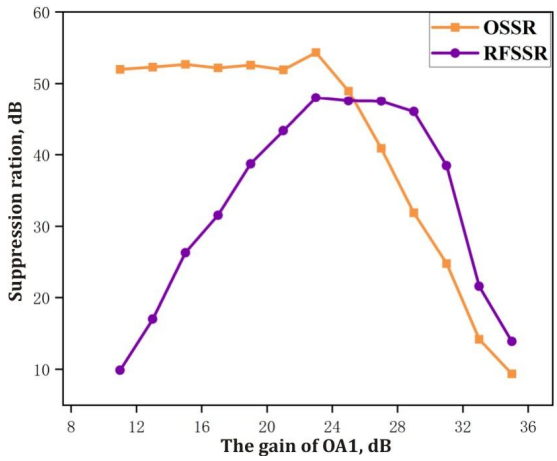

Fig. 5. *OSSR* and *RFSSR* versus gain of OA1.

3.2.2. Effect of Half-Wave Voltage of MZM5 on System Stability. The design value of the half-wave voltage for MZM5 in the system is 4 V. When the half-wave voltage of MZM5 varies between 2.5 V and 7.5 V, the relationship between *OSSR*, *RFSSR*, and the half-wave voltage is determined through sweeping parameter experiments, as shown in Fig. 6.

When the half-wave voltage of MZM5 increases from 2.5 V to 4 V, the *OSSR* rises from 20.24 dB to 53.33 dB. When it then increases from 4 V to 7.5 V, the *OSSR* decreases from 53.33 dB to 31.92 dB. If the half-wave voltage is 1 V lower than the design value, meaning a 25% deviation, the *RFSSR* is 17.41 dB. Conversely, if the voltage exceeds the design value by 2.5 V, representing a 62.5% deviation, the *RFSSR* is 21.04 dB. Therefore, when the half-wave voltage of MZM5 is between 25% and 62.5% above or below the set value, the second-order modulation's modulation index will be affected, which in turn impacts the sideband amplitude of the MZM5 output.

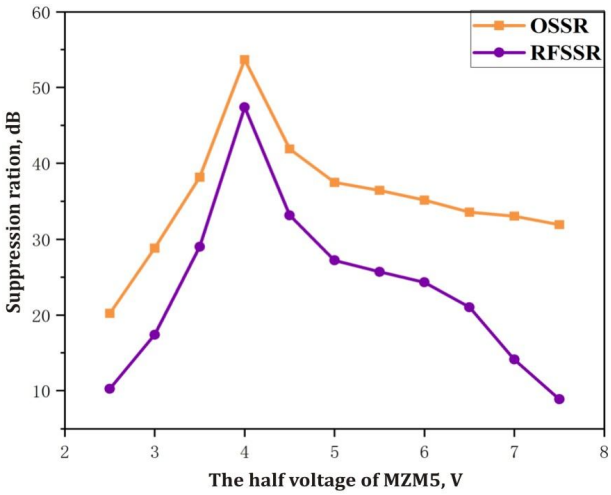

Fig. 6. *OSSR* and *RFSSR* versus half-wave voltage of MZM5.

3.2.3. Effect of modulation index on system stability. The design value of the modulation index for the first modulation in the system is 8.65. When the modulation index varies within 0.1 below and 0.1 above the design value, the relationship between *OSSR*, *RFSSR*, and the modulation index is determined through sweep parameter experiments as shown in Fig. 7.

When the modulation index is below the designed value of 0.1, the *OSSR* drops from 53.33 dB to 20.86 dB, and the *RFSSR* decreases from 47.98 dB to 13.46 dB. When the modulation index exceeds 0.1, the *OSSR* decreases from 53.33 dB to 20.17 dB, and the *RFSSR* drops from 47.98 dB to 13.57 dB. If the modulation index falls below 0.075, the corresponding *OSSR* and *RFSSR* are 23.62 dB and 16.77 dB, respectively. When it is above 0.075, they are 23.34 dB and 17.47 dB. Therefore, the modulation index should not vary more than 87% from the design value, or it will influence the sideband amplitude of the first modulation output.

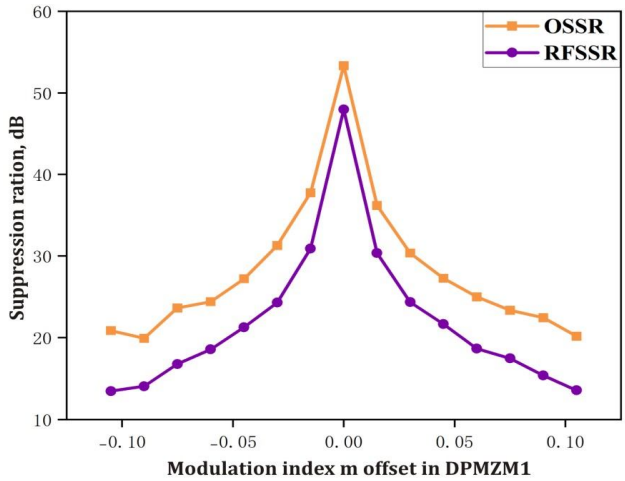

Fig. 7. Effect of modulation index on *OSSR* and *RFSSR* of the first modulation output.

3.2.4. Effect of extinction ratio on OSSR and RFSSR. Fig. 8a shows how the signal *OSSR* and *RFSSR* change when the extinction ratio varies from 10 dB to 100 dB in DPMZM1 and DPMZM2. It is

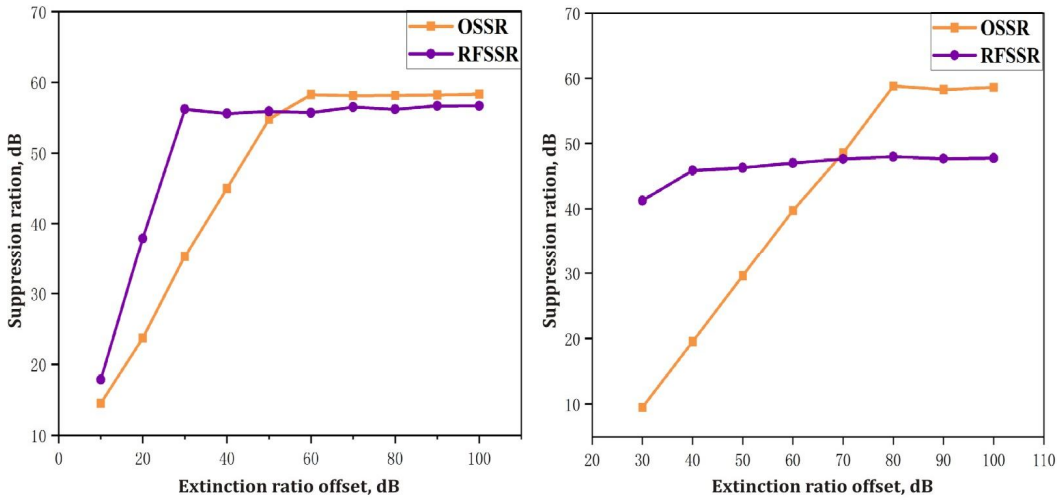

Fig. 8. Effect of extinction ratio on *OSSR* and *RFSSR* for the first modulation (a) and for the second modulation (b).

evident that when the extinction ratio ranges from 10 dB to 60 dB, both *OSSR* and *RFSSR* increase as the extinction ratio rises. Beyond 60 dB, the growth of *OSSR* and RFSSR becomes very slow. Fig. 8b illustrates the effect of extinction ratio on signal *OSSR* and *RFSSR* in MZM5 when varied from 30 dB to 100 dB. It can be observed that in the range of 30 dB to 80 dB, the suppression of the ±16th-order optical band for the 0th-order component increases with the extinction ratio, and *OSSR* rises gradually once the extinction ratio exceeds 80 dB. At an extinction ratio of 40 dB, the *OSSR* and *RFSSR* are 19.52 dB and 45.86 dB, respectively, meeting transmission requirements. When the extinction ratio is varied from 40 dB to 100 dB, *RFSSR* increases slowly as the extinction ratio increases. To ensure high purity of the modulated signal and prevent interference from spurious modulation, *RFSSR* should be kept above 40 dB. Therefore, the extinction ratio should be set above 20 dB whenever possible.

3.2.5. Effect of DC bias of MZM on OSSR and RFSSR. Fig. 9 shows how DC bias affects *OSSR* and RFSSR. The impact of DC bias during the first modulation on *OSSR* and *RFSSR* is shown in Fig. 9a, while Fig. 9b shows the effects during the second modulation. It is clear that both

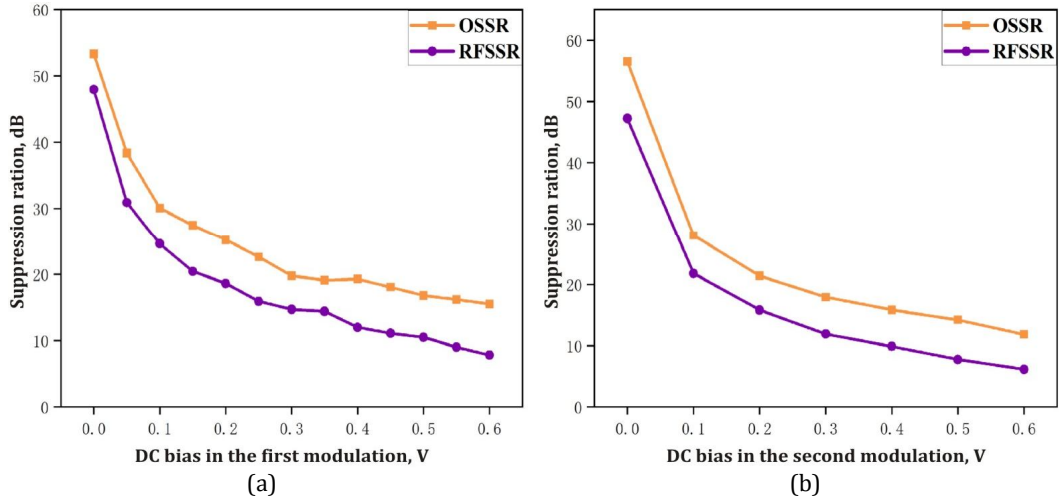

Fig. 9. Effect of DC bias on *OSSR* and *RFSSR* in the first modulation (a) and during the second modulation (b).

OSSR and RFSSR decrease as the DC bias drift increases. Additionally, from Figs. 9a and 9b, it is evident that when the DC bias drift in the first modulation stays within 0.2 V and in the second modulation within 0.1 V, *OSSR* and *RFSSR* stay above 25 dB and 18 dB, respectively, meeting the transmission requirements.

4. Transmission performance verification

To verify the transmission performance of the proposed 32-fold frequency millimeter-wave generation scheme, we construct a basic radio over fiber (RoF) transmission link, as shown in Fig. 10. In this setup, the 2.5 Gbit/s non-null-code baseband data signal is modulated onto the ±16th-order optical sideband using an MZM, and the modulated output spectrum is shown in Fig. 11a. This signal is then transmitted to PD3 through a single-mode fiber (SMF) to complete the frequency doubling process, with the output spectrum displayed in Fig. 11b. The output signal primarily consists of a 160 GHz millimeter wave signal and a baseband data signal. As shown in Figs. 13 and 14, to evaluate the transmission performance of the proposed scheme, the variation of bit-error-rate (BER) and Q-factor with received power is analyzed for back-to-back (BTB) transmission over 15 km.

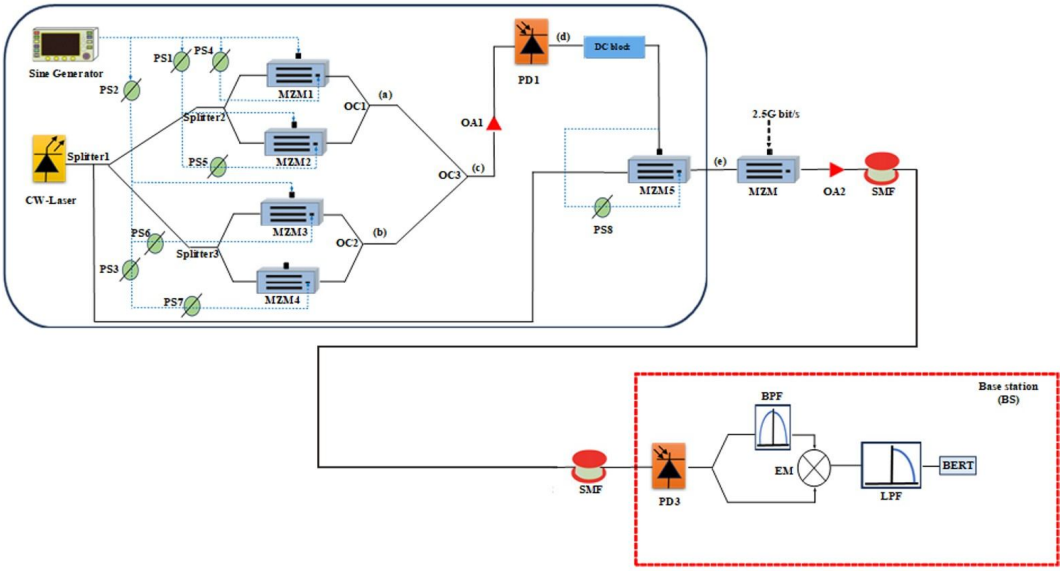

Fig. 10. The basic RoF transmission link: BPF - bandpass filter; LPF - low-pass filter; BS - base station; BERT - BER test; SMF – single-mode fiber; EM - electrical multiplier.

From Fig. 11a, it can be observed that the 2.5 Gbit/s downlink data is modulated onto the ±16th-order sideband. Fig. 11b shows the output spectrum after PD3 detection, where the main output signal is a 160 GHz millimeter-wave signal modulated with the baseband data. As illustrated in Figs. 12 and 13, to verify the transmission performance of the proposed scheme, both back-to-back (BTB) transmission and 15-km standard single-mode fiber transmission are conducted on the 2.5 Gbit/s baseband signal modulated onto the system-generated millimeter-wave signal. These tests analyze how the signal's BER and Q-factor vary with different received optical powers. The baseband signal is detected by a PD3 and then demodulated to measure the BER and Q-factor, using a BER tester at various received optical powers. The standard single-mode fiber has an attenuation of 0.2 dB/km and dispersion of 16.75 ps/nm·km. In Fig. 12, it is evident that the BER decreases as the

received power increases. From Fig. 13, it is clear that the Q-factor improves with increasing input optical power. Fig. 14 displays the eye diagram after BTB and 15-km fiber transmission. When the received optical power is -15.3 dBm, the BER reaches 10^{-17}, matching the BER for the 15 km fiber transmission. Despite dispersion and linear chirp affecting the 16th-order optical sideband after 15 km of fiber transmission, the eye diagram still maintains a good shape.

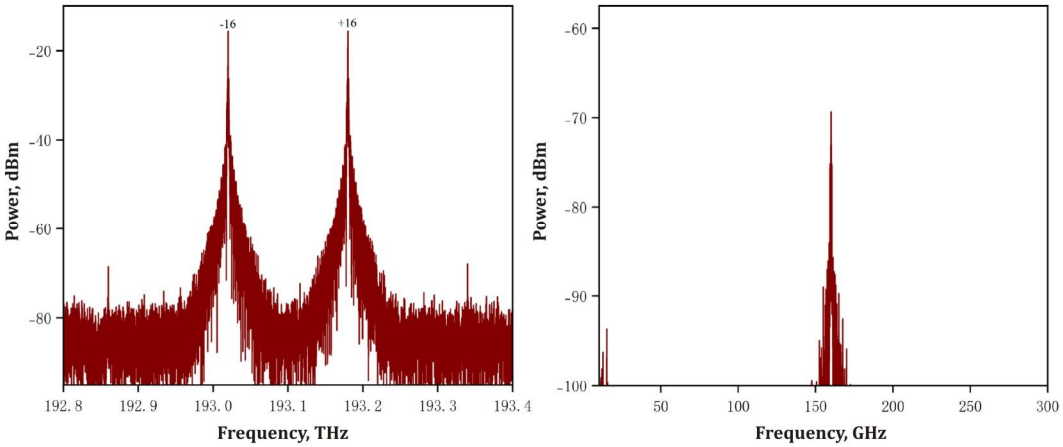

(a) (b)

Fig. 11. (a) MZM modulation output spectrum, (b) PD3 output millimeter wave signal spectrum.

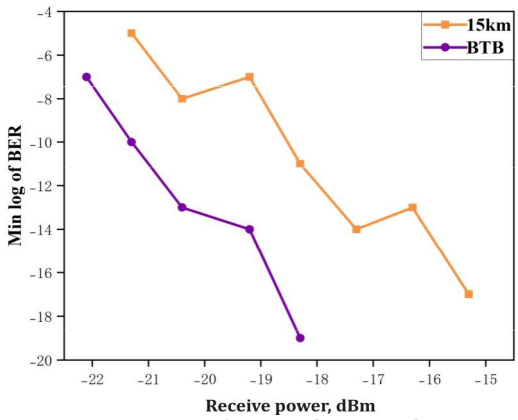

Fig. 12. Variation of BER with received power.

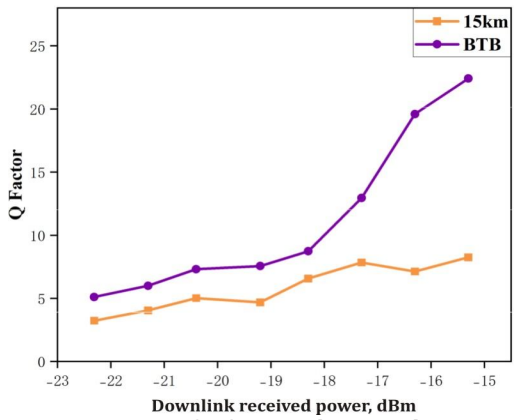

Fig. 13. Variation of Q-factor with received power.

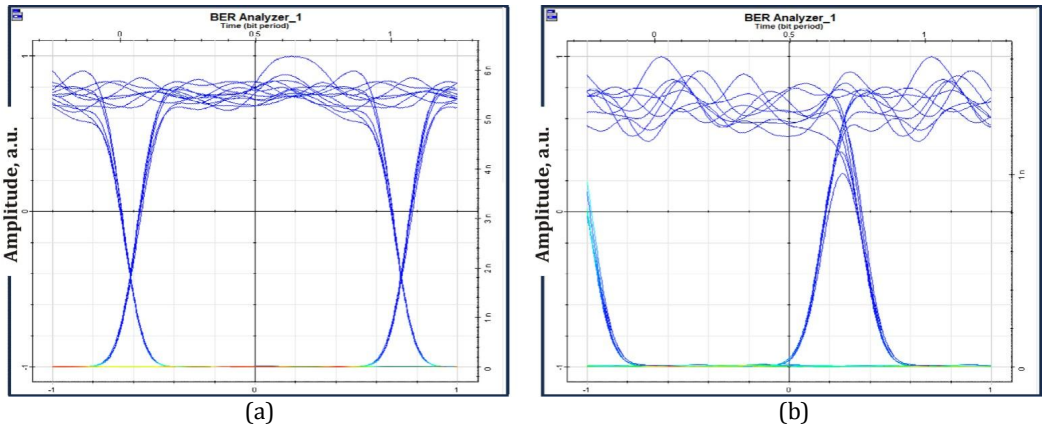

(a) (b)

Fig. 14. Eye diagrams after BTB transmission (a) and after 15 km of fiber transmission (b).

5. Conclusion

This paper proposes a new method using five MZMs to generate 32-fold millimeter wave signals by modulation, aiming to produce 160 GHz MMW signals from 5 GHz signals. The system's structure is explained in detail, and its feasibility is confirmed through theoretical analysis and simulation. The system results were optimized by adjusting the modulation index m of the Mach-Zehnder modulator, the electric phase shifter, and the optical amplifier's parameters. The simulation results demonstrate that the *OSSR* and *RFSSR* of the 160 GHz millimeter waves produced by this method are, respectively, 53.33 dB and 47.98 dB, aligning with the theoretical calculations. To assess the system's stability, the effects of various parameter variations under non-ideal conditions were analyzed, including: the extinction ratios of DPMZM1, DPMZM2, and MZM3 exceeding 40 dB; the deviation of the modulation index m in DPMZM1 and DPMZM2 being less than 87% of the design value; the half-wave voltage of MZM3 being at least 25% of the set value and not exceeding 62.5%; and the gain deviation of OA1 remaining within 43.48% of the design value. Under these conditions, the quality of the generated MMW signal meets real-world transmission requirements. Finally, the system's transmission performance was tested over 15 km of single-mode fiber with a BER of 10^{-17}. Therefore, in practical applications, preprocessing of input modulation signals of different formats is necessary to eliminate phase noise's impact on transmission performance [38]. The scheme's advantages include a simple structure and a high multiplication factor, making it suitable for use in current or future communication systems.

Funding. This research work was supported in part by the Scientific Research Project of Fuyang Normal University (2022KYQD0004) and the Anhui Education Department, and the University Natural Science Research Project of Anhui Province (Grant No.: 2022AH051338). This work is supported by Henan Key Laboratory of Visible Light Communications (No. HKLVLC2023-B10), Jiangxi Provincial Natural Science Foundation (20232BAB212006, 20242BAB20041), and Open Fund of Advanced Cryptography and System Security Key Laboratory of Sichuan Province (Grant No. SKLACSS-202303, Grant No. SKLACSS-202306). Anhui Digital Intelligent Engineering Research Center for Agricultural Products Quality Safety (APDI202302). This work is supported by Hubei Provincial Natural Science Foundation of China (Grant No: 2023AFB474, Grant No: 2024AFB881), and Postgraduate Quality Engineering Project of Anhui Province (Grant No: 2024jyjxggyjY232). This work is supported by the Chinese Institute of Electronic Labor (CIEL) Educational Reform and Development Projects (Grant No: Ceal2024136, Grant No: Ceal2024137).

Conflicts of interest. The authors declare that they have no known competing financial interests or personal relationships that could have appeared to influence the work reported in this paper.

References

1. Yang, Y., Yamagami, Y., Yu, X., Pitchappa, P., Webber, J., Zhang, B., Fujita, M., Nagatsuma, T. & Singh, R. (2020). Terahertz topological photonics for on-chip communication. *Nature Photonics*, *14*(7), 446-451.
2. Li, J., Ning, T., Pei, L., Qi, C., Hu, X., & Zhou, Q. (2010). Photonic frequency-quadrupling scheme for millimeter-wave generation by employing feed-forward modulation technique. *Optics Express*, *18*(3), 2503-2508.
3. Novak, D., Waterhouse, R. B., Nirmalathas, A., Lim, C., Gamage, P. A., Clark, T. R., Dennis, M.L. & Nanzer, J. A. (2015). Radio-over-fiber technologies for emerging wireless systems. *IEEE Journal of Quantum Electronics*, *52*(1), 1-11.

4. Chen, S., & Zhao, J. (2014). The requirements, challenges, and technologies for 5G of terrestrial mobile telecommunication. *IEEE Communications Magazine*, *52*(5), 36-43.
5. Han, Y. S., Zheng, Z., Luo, Z., Min, Z., Xu, O., & Liu, J. (2015). High-power optical millimeter-wave signal generation with tunable frequency multiplication factor. *Optics Communications*, *335*, 53-59.
6. Cai, X., Cheng, X., & Tufvesson, F. (2024). Toward 6G with terahertz communications: Understanding the propagation channels. *IEEE Communications Magazine*, *62*(2), 32-38.
7. Sung, M., Kim, S., Kim, E. S., Moon, S. R., Kim, M., Lee, I. M., Park, K.H., Lee, J.K. & Cho, S. H. (2023). Photonic THz communications based on radio-over-fiber technology for 6G mobile network: Design and opportunity. *IEEE Journal of Selected Topics in Quantum Electronics*, *29*(5: Terahertz Photonics), 1-11.
8. Pi, Z., & Khan, F. (2011). An introduction to millimeter-wave mobile broadband systems. *IEEE Communications Magazine*, *49*(6), 101-107.
9. Chen, L., Pi, Y., Wen, H., & Wen, S. (2007). All-optical mm-wave generation by using direct-modulation DFB laser and external modulator. *Microwave and Optical Technology Letters*, *49*(6), 1265-1267.
10. Xu, H., Venkatasubramani, L. N., Chaudhuri, R. B., Browning, C., Yu, Y., & Barry, L. P. (2023). Fabry-Pérot optical frequency comb based mm-wave RoF system using pilot-assisted equalizer. *Optics Express*, *31*(19), 30947-30960.
11. Wang, H., & Li, X. (2018, April). Vector mm-wave signal generation at W-band based on EAM+ PM. In *Metro and Data Center Optical Networks and Short-Reach Links* (Vol. 10560, pp. 183-193). SPIE.
12. Wang, D., Wang, X., Yang, X., Gao, F., Zhang, L., Yang, Z., & Wu, B. (2023). Photonic filter-free adjustable frequency sextupling scheme for V-band vector mm-wave signal generation based on a DP-MZM with precoding. *Optics Communications*, *545*, 129633.
13. Abouelez, A. E. (2020). Optical millimeter-wave generation via frequency octupling circuit based on two parallel dual-parallel polarization modulators. *Optical and Quantum Electronics*, *52*(10), 439.
14. Hasanuzzaman, G. K. M., Kanno, A., Dat, P. T., & Iezekiel, S. (2018). Self-oscillating optical frequency comb: Application to low phase noise millimeter wave generation and radio-over-fiber link. *Journal of Lightwave Technology*, *36*(19), 4535-4542.
15. Liu, G., Lu, Z., Liu, J., Poole, P. J., Mao, Y., Xie, X., Vachon, M. Song, C.-Y. & Barrios, P. (2024, March). Directly modulated quantum-dash mode-locked lasers for millimeter-wave over fiber applications. In *Terahertz, RF, Millimeter, and Submillimeter-Wave Technology and Applications XVII* (Vol. 12885, pp. 137-140). SPIE.
16. Yu, J., Jia, Z., Yi, L., Su, Y., Chang, G. K., & Wang, T. (2006). Optical millimeter-wave generation or up-conversion using external modulators. *IEEE Photonics Technology Letters*, *18*(1), 265-267.
17. Thomas, V. A., El-Hajjar, M., & Hanzo, L. (2015). Millimeter-wave radio over fiber optical upconversion techniques relying on link nonlinearity. *IEEE Communications Surveys & Tutorials*, *18*(1), 29-53.
18. Thomas, V. A., El-Hajjar, M., & Hanzo, L. (2015). Millimeter-wave radio over fiber optical upconversion techniques relying on link nonlinearity. *IEEE Communications Surveys & Tutorials*, *18*(1), 29-53.
19. Chen, H. Y., Chi, Y. C., Lin, C. Y., Tsai, C. T., & Lin, G. R. (2016). Four-wave-mixing suppression of master-to-slave injection-locked two-wavelength FPLD pair for MMW-PON. *Journal of Lightwave Technology*, *34*(20), 4810-4818.
20. Aghighi, A., Essawy, M., & Natarajan, A. S. (2024). A frequency doubler with second harmonic feedback for wideband, efficient frequency multiplication at millimeter-wave. *IEEE Transactions on Microwave Theory and Techniques*, *72*(5), 2704-2715.
21. Chung, A., Rejeb, M. B., Darwish, A., Hung, H. A., & Boumaiza, S. (2018, September). Frequency doubler based outphasing system for millimeter wave vector signal generation. In *2018 15th European Radar Conference (EuRAD)* (pp. 449-452). IEEE.
22. Tao, L. B., Gao, H. Y., Deng, S., Lü, H. F., Wen, X. Y., & Li, M. (2020). A simplified optical millimeter-wave generation scheme based on frequency-quadrupling. *Optoelectronics Letters*, *16*(1), 7-11.
23. Xu, W., Gao, X., Zhao, M., Xie, M., & Huang, S. (2018). Full duplex radio over fiber system with frequency quadrupled millimeter-wave signal generation based on polarization multiplexing. *Optics & Laser Technology*, *103*, 267-271.
24. Chen, X. (2020). Improved filterless sextupling optical MM-wave generation and RoF transmission. *Optik*, *206*, 164337.
25. Shen, S., & Yin, W. (2018). Photonic generation of high-purity 60 GHz millimeter-wave signal requiring only 10 GHz radio frequency local oscillator. *Optical Review*, *25*(6), 684-693.
26. Hasan, M., & Hall, T. J. (2016). A photonic frequency octo-tupler with reduced RF drive power and extended spurious sideband suppression. *Optics & Laser Technology*, *81*, 115-121.
27. Zhu, Z., Zhao, S., Li, X., Qu, K., & Lin, T. (2017). Filter-free photonic frequency sextupler operated over a wide range of modulation index. *Optics & Laser Technology*, *90*, 144-148.

28. Zhu, Z., Zhao, S., Li, Y., Chen, X., & Li, X. (2015). A novel scheme for high-quality 120 GHz optical millimeter-wave generation without optical filter. *Optics & Laser Technology*, *65*, 29-35.
29. Chen, X., Dai, S., Li, Z., Xiao, H., Zhang, L., & Chen, X. (2024). Study of the generation of two frequency 16-tupling millimeter wave and transmission over fiber by remodulation with Mach–Zehnder modulators. *Optical and Quantum Electronics*, *56*(4), 539.
30. Chen, X., Li, Z., Ba, W., Dai, S., Liang, J., & Xiao, H. (2023). A novel method to generate and transmit 40-tupling frequency millimeter wave over fiber based on remodulation of MZMs. *Heliyon*, *9*(3).
31. Rani, A., & Kedia, D. (2023). An 18-tupled photonic millimeter-wave generation using cascaded Mach-Zehnder modulators. *Fiber and Integrated Optics*, *42*(1), 1-19.
32. Chen, X., Xia, L., & Huang, D. (2017). A filterless 24-tupling optical millimeter-wave generation and RoF distribution. *Optik*, *147*, 22-26.
33. Chen, X., Dai, S., Li, Z., Ba, W., & Chen, X. (2024). Thirty-two-tupling frequency millimeter-wave generation based on eight Mach–Zehnder modulators connected in parallel. *ETRI Journal*, *46*(2), 194-204.
34. Chen, X., Chen, X., Dai, S., Li, B., & Wang, L. (2024). A novel frequency 32-tupling ROF system without bit walk-off effect based on MZM with inserting pilot. *Heliyon*, *10*(12).
35. Shang, Y. B., Lin, X. D., Xia, G. Q., & Wu, Z. M. (2022, December). Simulation study on the high-quality 32-tupling millimeter-wave signal generation based on a filter-free photonic scheme with four DP-MZMs. In *Semiconductor Lasers and Applications XII* (Vol. 12311, pp. 189-197). SPIE.
36. Chen, X., Dai, S., Li, Z., Liu, X., Chen, X., & Xiao, H. (2023). Filterless frequency 32-tupling millimeter-wave generation based on two cascaded dual-parallel Mach–Zehnder modulators. *Frontiers in Physics*, *11*, 1212482.
37. Zhu, Z., Zhao, S., Zheng, W., Wang, W., & Lin, B. (2015). Filterless frequency 12-tupling optical millimeter-wave generation using two cascaded dual-parallel Mach–Zehnder modulators. *Applied Optics*, *54*(32), 9432-9440.
38. Wang, D. (2022). W band vector millimeter-wave signal generation based on a new photonic frequency quadrupling without optical filter. *Microwave and Optical Technology Letters*, *64*(7), 1204-1209.

Yang Cui, Dongfei Wang, Xiangqing Wang, Xiaokun Yang, Jiahui Wang, Daisheng Zhang. (2025). Mechanism for 32-Fold Frequency Multiplication Terahertz Wave Generation Based on Two Dual-Parallel and One Cascaded MZMs Without Filtering for High-Frequency Communications**.** *Ukrainian Journal of Physical Optics*, *26*(4), 04032 – 04048.
doi: 10.3116/16091833/Ukr.J.Phys.Opt.2025.04032

Анотація*. У цій статті представлено схему генерації міліметрових хвиль з 32×кратною частотою за допомогою вторинної модуляції без фільтрів, що базується на п'яти модуляторах Маха-Цендера (ММЦ). Система керується радіочастотним (РЧ) сигналом 5 ГГц. Кожен з двох подвійно-паралельних ММЦ містить два ММЦ, що працюють паралельно. Перша модуляція створює РЧ-сигнал 80 ГГц для другої модуляції. Після проходження через блокувальний модуль постійного струму каскадний ММЦ виконує вторинну модуляцію для генерації оптичних бічних смуг ±16-го порядку. Нарешті, 32×множення частоти досягається через частоту биття на фотодетекторі. Теоретичний аналіз та експерименти з моделювання показують, що коефіцієнт придушення оптичної бічної смуги системи становить 53,33 дБ, а коефіцієнт придушення РЧ бічної смуги - 47,98 дБ. Ці узгоджені результати підтверджують доцільність схеми. Вплив неідеальних факторів ММЦ на стабільність системи досліджується за допомогою моделювання, і наводяться їх допустимі діапазони. Зрештою, результати моделювання показують, що коефіцієнт помилок бітів залишається нижче 10^{-9} під час передачі сигналів міліметрових хвиль зі швидкістю 2,5 Гбіт/с, модульованих у базовій смузі, на відстань 15 км в оптичному волокні. Ця схема має просту структуру та коефіцієнт множення високої частоти, що пропонує перспективні застосування в технології міліметрових хвиль.*

Ключові слова*: міліметрова хвиля, модулятор Маха-Цендера, коефіцієнт приглушення бічної смуги радіочастот, коефіцієнт приглушення оптичної бічної смуги, передача міліметрової хвилі по оптичному волокну, 32-кратне множення частоти*